CHAPTER V

OPTICAL CHARACTERIZATION OF ALIGNED QUANTUM DOTS

5.1 Self-Assembly Crystal Growth

The quantum dots characterized in this thesis were produced by the crystal-growth method of molecular-beam epitaxy (MBE). In MBE, one begins with a high-quality substrate, heated and placed in an ultra-high vacuum. Sources of pure elements are heated so that a small flux of atoms evaporates and goes towards the substrate as a beam. These beams are turned on and off using shutters. Some of the atoms that strike the substrate stick to it, and due to the high temperature of the substrate, these atoms move across the surface until they find an energetically favorable resting place, typically along an atomic step. These steps propagate across the sample surface as single monolayers which are deposited onto the substrate. Optimal crystal growth depends on the atomic beam flux ratios, the substrate temperature, and the absence of contaminants.

The self-assembled InAs quantum dots illustrated in Fig. 5.1 was grown by technique known as Stranski-Krastanov growth mode [66]. Here, quantum dots form when InAs is grown on top of GaAs, due to the lattice size mismatch (the natural lattice size of InAs is 7% larger). The first one or two monolayers of InAs match the underlying GaAs lattice, but are under mechanical strain. This initial, smooth layer of InAs is called the "wetting layer." After a critical thickness (typically less than 2 monolayers), it becomes energetically favorable for the InAs layer to form islands. These are typically 4-7 nm thick and 20-40 nm in diameter, depending on the growth parameters. The density of islands depends on both the growth temperature and the amount of indium deposited, which can vary from 10 μm^{-2} to 500 μm^{-2}. By the aid of atomic-force microscope (AFM) images, surface morphology of uncapped InAs islands may be seen. For optical characterization of the quantum dot structures, a GaAs capping layer is grown on top.

The optical properties of quantum dots depend heavily on the growth process. The emission wavelength depends on both the size and the composition (how much GaAs is mixed into the InAs island). The eigen-energy-level spacings for these quantum structures also depend on these same factors. The fine structure splitting

depends on the amount of asymmetry in the shape of the structure and in the associated strain field [67]. The cleanliness of the growth might affect whether quantum dots start out neutral, or with extra charges.

In this chapter the optical characterizations of ordered quantum dots which were grown by using the thin-capping-and-regrowth technique and on virtual substrates are addressed.

5.2 Thin-Capping-and-Regrowth Technique

Recently, ordered InAs QDs grown on GaAs [001] substrate using a thin-capping-and-regrowth technique have been demonstrated [68]. First, the randomly distributed QDs were grown on a flat surface by using conventional growth technique. A thin GaAs layer was then capped on top of the QD layer. Because of the lattice mismatch between the QDs and the capping layer, the strain energy around the QDs is increased and In atoms migrate out from the QDs. As a result, a nano-hole appeared in the middle of each QD. By regrowing the QDs on the top of the nano-holes via the thin-capping process, nano-propeller QDs were formed. By repeating the thin-cap-and-regrowth method for three cycles, QDs thus formed aligned along in one direction, specifically the $[1\bar{1}0]$ direction. The following section discusses the optical characterizations of such aligned quantum dots, but the optical characterizations of as-grown QDs and of very-high-density QDs will be presented first, serving as the reference.

5.2.1 (a) As-grown QDs (Reference Sample)

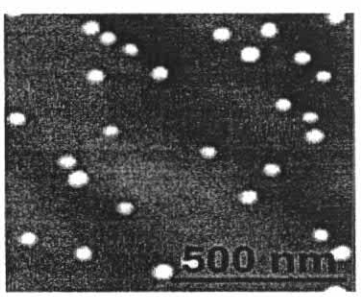

Figure 5.1 AFM image of as-grown InAs QDs grown on semi-insulating [001] GaAs substrate. (Suraprapapich *et al.*, 2005)

According to AFM images, the as-grown InAs QDs are randomly distributed on the sample surface. The size of QDs appearing on the AFM images, is almost circular. For the optical characterization, two PL peaks were observed, as shown in Fig.5.2, and no polarization property was observed.

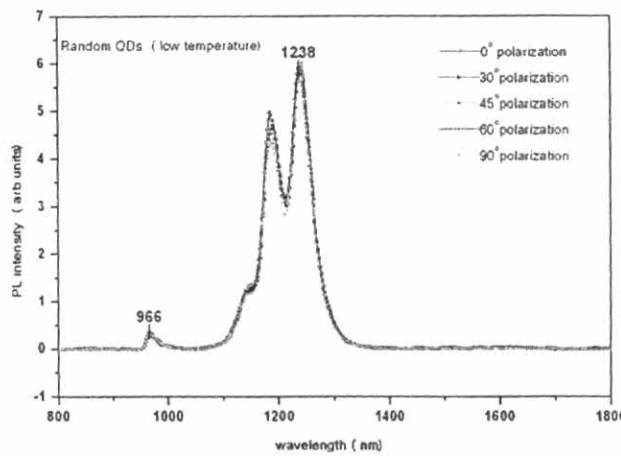

Figure 5.2 Polarization-resolved PL spectra of as-grown InAs QDs measured at 77 K.

5.2.1 (b) High-density QDs (Reference Sample)

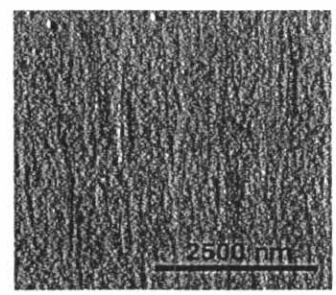

Figure 5.3 AFM image of high-density InAs QDs on semi-insulating [001] GaAs substrate grown by using the thin-capping-and-regrowth technique for 10 cycles. (Suraprapapich *et al.*, 2005)

According to AFM images, the InAs QDs are densely distributed on the sample surface. The actual size of the QDs is difficult to evaluate from the AFM images. The dot size uniformity is worse than the previous sample because of the high dot density. As expected, in optical characterization, a broad spectrum with no polarization characteristic was observed for this sample. Very small emission intensity difference

between parallel and perpendicular directions may come from the error of optics, which is about 0 - 4 %.

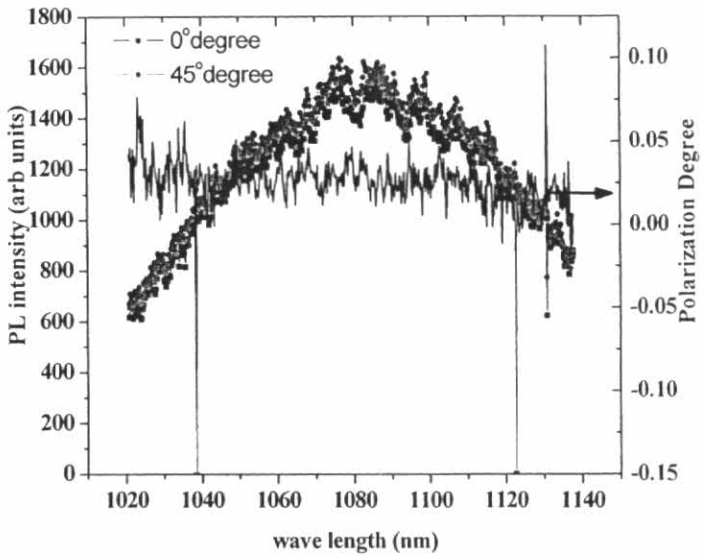

Figure 5.4 PL spectra of high-density InAs QDs measured at a low temperature (4 K) with the excitation power of 500 μW.

Table. 5.1: Summary of the optical characterization of as-grown QDs and high-density QDs.

	Peak (eV)		**FWHM (meV)**	
Temperature	RT	77 K	RT	77 K
As-grown QDs	0.992	1.01	29	28
High-density QDs	1.13	1.148	100	96

5.2.2 Binary Quantum Dots

When two semiconductor QDs are close to each other, carriers in the QDs begin to interact with one another. In particular, the wavefunctions of the carriers in the binary-QD system may overlap. Coupled quantum dots have been interested because of coupling and entanglement of quantized energy states between neighboring QDs. They possess a potential application for quantum information devices [69]. The formation of laterally coupled binary quantum dots may be achieved on the [001] GaAs substrate by gas-source MBE (GSMBE). First, a 300-nm GaAs buffer layer was deposited at 580°C, followed by a 1.8 ML of InAs QDs after reducing a substrate temperature to 500°C. Then the substrate temperature was reduced to 470°C and a 6 ML of thin GaAs capping layer was-grown on the randomly distributed QD layer. A similar routine leads to the modification of nano-templates for formation of quantum rings (QRs). At a regrowth thickness of 0.6 ML, binary quantum-dot molecules (Bi-QDMs) are formed at the rims of QRs on which preferable sites for quantum dots in the molecules to form are aligned along in $[1\bar{1}0]$ direction [70].

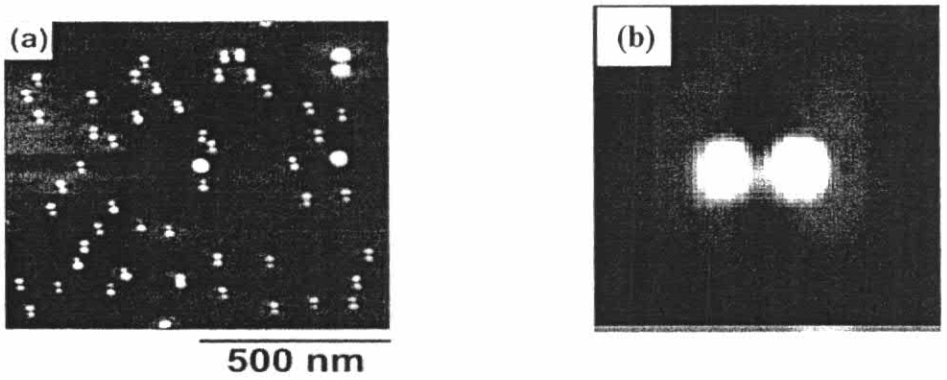

Figure 5.5 (a) AFM image of binary QDs, and (b) close-up image of binary QDs. (Suraprapapich *et al.*, 2006)

According to AFM information, the two quantum dots are close together and the center-to-center distance between two QDs is 22 nm, the size of individual QDs on Bi-QDs is 20 nm, so that this system can be regarded as coupled quantum dots. The coupling effect in bi-QDs is expected to affect the optical properties of the structure. With the aid of photoluminescence spectroscopy, information about electronic levels

of these structures was subsequently investigated. Additional information from the polarization measurement results supports to learn the physics of this kind of nanostructure. In this section the average information of the sample and individual quantum dots are investigated using micro-photoluminescence. The coupling behavior of InAs bi-QDs are presented by means of temperature-dependent PL, excitation-power-dependent PL, and polarized PL measurements. Conventional PL measurements and polarized PL measurements were also performed for individual quantum dots in the bi-QD system.

5.2.2.1 Excitation-Power-Dependent PL Measurements

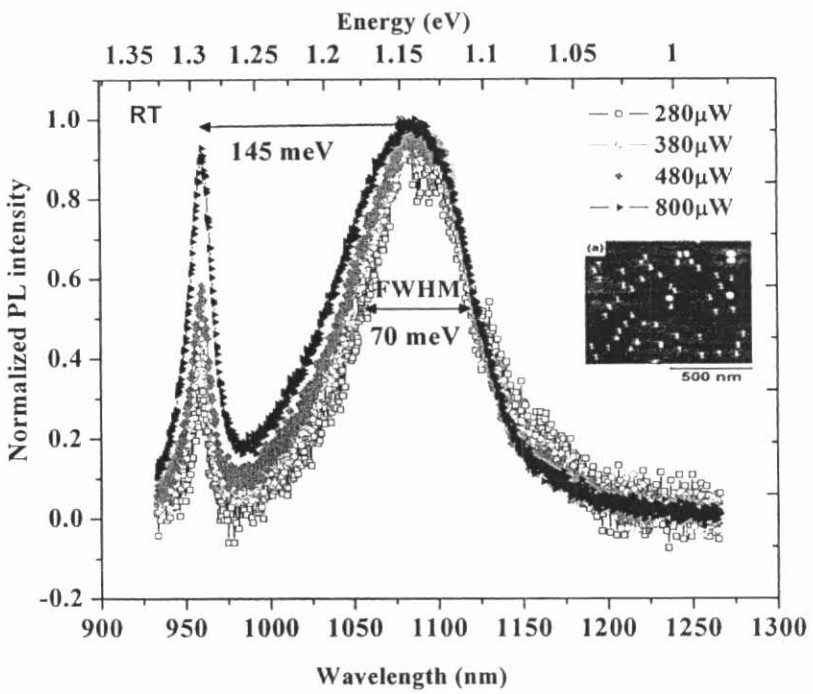

Figure 5.6 Excitation-power-dependent PL spectra of bi-QDs at room temperature.

Figure 5.6 shows various PL spectra at room temperature by using the laser excitation power ranging from 280 μW to 800 μW. The PL peak at 1100 nm (1.15 eV) was observed and the second peak around 953 nm (1.3 eV) distinctly occurred. The energy difference between the first peak and the second peak of about 145 meV is so large that it can not be considered as the excited state of QDs compared with typically 50-60 meV energy difference between the ground state and the excited state for isolated InAs quantum dots [71]. The second peak at 1.3 eV is attributed to the wetting layer of InAs quantum dots. A full-width-at-half-maximum (FWHM) of

around 70 meV is due to the size fluctuation and the thermal relaxation of carriers of QDs at a high temperature [72]. Strong PL intensity obtained for room-temperature measurement indicates that this structure can be utilized in light emitting device for room-temperature application.

To understand the physics of the bi-QD structure, low-temperature PL measurements were also carried out. At 10 K, the sample was excited by using different excitation powers as shown in Fig. 5.7. The PL spectrum can be fitted into two-Gaussian curves. To extract the two peaks out of the spectrum, the AFM images were then carefully investigated. The AFM images informed that the size of the bi-QDs is smaller than the single, isolated dots on the sample. Population of the smaller QDs (in bi-QDs) is 70% and that of merged QDs (larger size) is 30 % on this sample. The carrier confinement is better in smaller QDs and the luminescence intensity may be high. Thus, the peak at the higher energy side came from bi-QDs and the lower energy peak originated from merged singled QDs. The distance between the two peaks is around 60 meV. Further increasing the excitation powers lead to broader linewidths in the higher energy side, which is similar to the behavior observed from room-temperature measurement and is probably caused by the state filling effect [73]. Another consideration is that for uncorrelated QDs, state filling effect occurs at the first excited state of the QDs. Some literature reported experimentally that correlated quantum dots can give a broadened linewidth at the higher energy side. This kind of behavior is also observed in another coupled QDs sample [74].

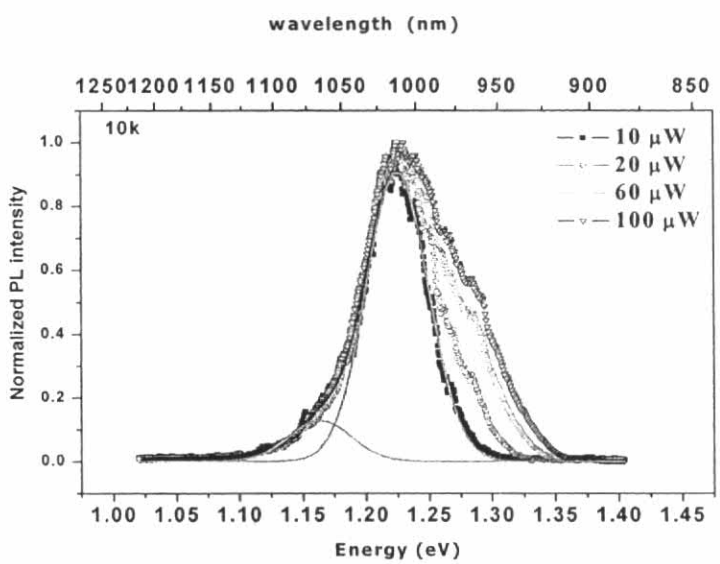

Figure 5.7 Excitation-power-dependent PL spectra at 10 K. The spectrum can be convoluted into two Gaussian peaks.

5.2.2.2 Temperature-Dependent PL Measurements

Figure 5.8 shows a temperature-dependent PL spectrum and Figure 5.9 shows the integrated PL intensity of bi-QDs. It is seen that: First, the PL spectral shape and the peak position are dependent on temperature. Second, the integrated PL intensity increases with the increasing temperature up to a certain temperature and then decreases with further increasing the temperature. In general, the PL intensity decreases with increasing temperature due to an enhancement of the non-radiative recombination process and a reduction of the excitonic transition with temperature [75]. One possible reason for an increase in the integrated PL intensity as well as a change of the peak position and the spectral linewidth is connected with the carrier dynamics [76]. In case of a coupled bi-QD system, the wavefunctions of the carriers in the adjacent QDs overlap with each other. This overlapping of wavefunctions is expected to relieve the phonon relaxation bottle neck by increasing the number of states related to carriers and so the integrated PL intensity increases with the increasing relaxation [77]. When the temperature goes up, the coupling and relaxation effect will increase because of the increasing electron-phonon interaction.

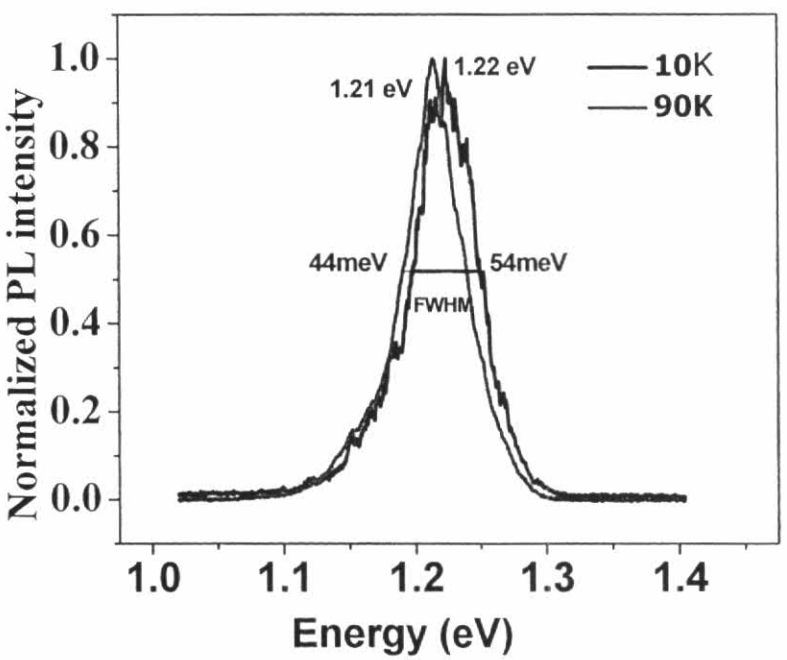

Figure 5.8 Temperature-dependent PL spectra of bi-QDs measured at 10 K and 90 K. The peak shift by 10 meV was clearly observed at 90 K.

As a result, the photogenerated carriers transfer and relax into the energetically lower energy state, and recombine there. Consequently, the PL peak is shifted to a lower energy level. Increasing photogenerated carriers in the lower energy level at higher temperature causes a higher PL intensity [78-79]. This process is also expected to cause a reduction in the FWHM of the PL spectrum. At 90 K, the integrated PL intensity is highest and the linewidth decreases to 44 meV compared with the 54 meV at 10 K. Further increasing the temperature, the linewidth increases again and the integrated PL intensity reduces. This is due to the electron-phonon scattering and thermal distribution [80].

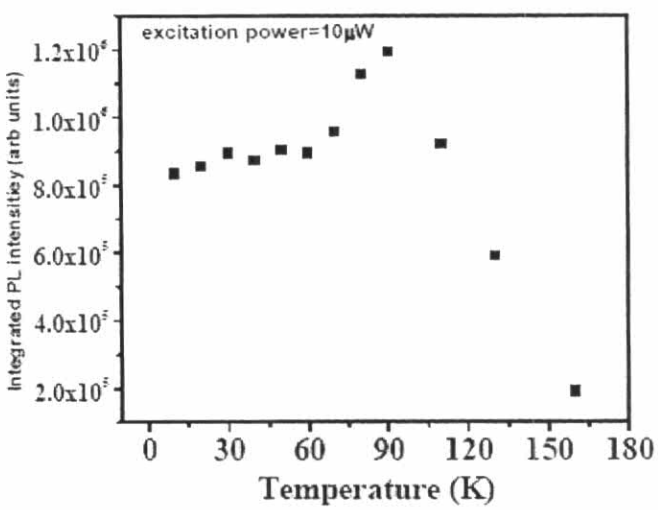

Figure 5.9 Temperature-dependent integrated PL intensity of bi-QDs. The temperature ranges from 4 K to 180 K, and the laser excitation power was held at 10 μW.

5.2.2.3 Polarization-Resolved PL Measurements

The polarization measurements were carried out to learn the detailed physics of the bi-QDs. At room-temperature measurement, the distinct linear polarization was not observed. At 10 K, the linear polarization degree was 7% and almost no polarization dependence was found for the PL emission from the GaAs substrate, however. The anisotropy was nearly constant over the whole energy spectrum indicating a homogenous uniform shape, orientation and strain distribution [81]. Further increasing the temperature, the polarization degree also increases, and at 50 K the polarization degree increases to a maximum value of 13%. Fig. 5.10 shows the

temperature-dependent polarization spectrum of bi-QDs, and Fig. 5.11 shows the polarization degree of bi-QDs change with the temperature. All polarization measurements were measured under non-resonant excitation in the barrier of GaAs and the detection time to measure the spectrum was 1 second.

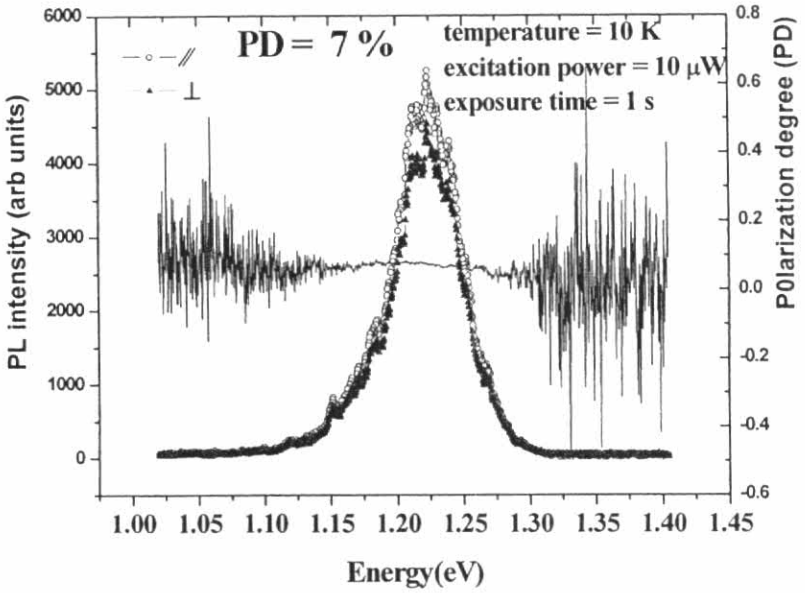

(a)

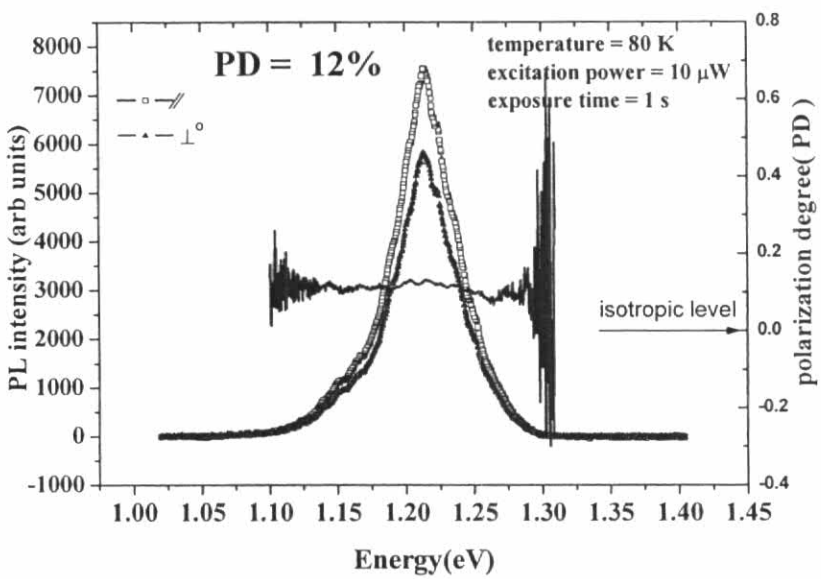

(b)

Figure 5.10 Temperature-dependent polarized PL spectra of binary QDs at (a) 10 K and (b) 80 K. When the temperature was increased, the shape of the spectrum changed and the polarization degree increased.

The temperature-dependent PL measurements show that the degree of linear polarization (PD) changes with the temperature. When temperature increases, the PD increases at first and attains the highest degree around 50 K. Between 50 K and 90 K, the polarization degree is almost constant, and above 90 K the polarization degree starts to decrease sharply. Therefore, the polarization degree in this binary QD is probably related to the carrier dynamics in the QDs [82]. This kind of polarization behavior is probably caused by the thermal dislocation of carriers from 0-D quantum dots state to the 2-D quantum well state with the increasing temperature. At low temperatures, the excitons are localized in the QDs. When the temperature was increased to a certain point, the localized carriers obtain enough energy to travel through the two coupled QDs. The coupling strength of the QDs becomes stronger and the QDs lost 0-D features and act like a 1-D quantum wire with an associated increase in polarization anisotropy [83]. When the temperature is high enough, optical polarization anisotropy is reduced. The mechanism of reducing PD is still unclear and need the some more experiments to decide the mechanism.

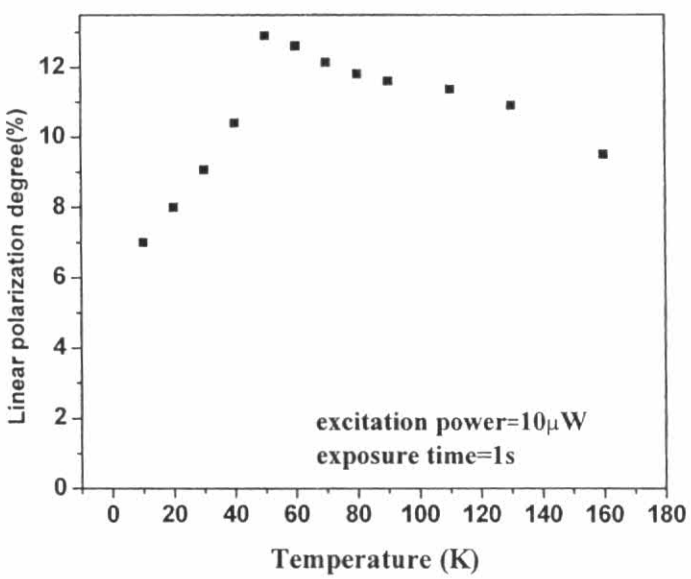

Figure 5.11 Temperature-dependent polarization degree of binary QDs; the temperature ranges from 4 K to 180 K, and the excitation power was held at 10 μW.

5.2.2.4 Single-Dot Spectroscopy

Optical spectroscopy studies of particular dot structures were performed to know the exact information of single QDs. The sample was held at 3.8 K in a continuous-flow cryostat. Individual PL spectra of single QD from the bi-QDs obtained under very low excitation power density while increasing the detection time into 90 s are shown in Fig. 5.12. At the lowest pump intensity, three emission peaks were observed at 1.133 eV, 1.135 eV and 1.136 eV, labeled as X1, X2 and X3, respectively. Usually, for a single dot, at low excitation power, only the exciton decay from the s-shell (shell with an orbital angular momentum L = 0) is observed. At high excitation powers, two or more excitons were present in any one dot. The origins of the peaks from the individual quantum dots were identified by measuring the power dependence of the spectra [84-86]. When the excitation power was increased, the spectral line X1, X2 and X3 increased with almost same intensity ratio. Another peak at around 1.134 eV appeared and was marked as XX.

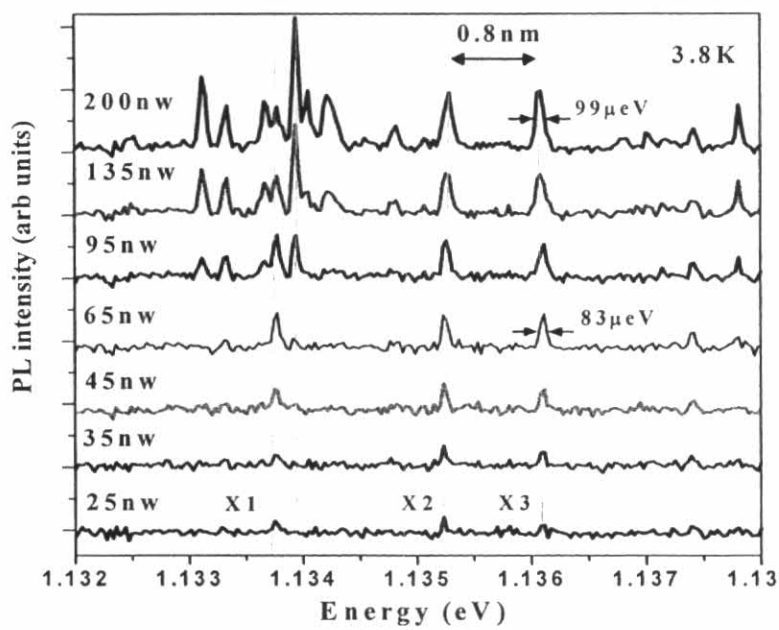

Figure 5.12 Excitation-power-dependent single-dot spectroscopy of the bi-QD system; the excitation power ranges from 25 nW to 200 nW, and the temperature was held at 3.8 K. At 25 nW, three distinct peaks were observed, and when the excitation power was increased, many peaks appeared.

The PL intensity as a function of excitation power is shown in Fig. 5.13. While the fundamental peak X1, X2 and X3 increases linearly with increasing excitation power, the additional peak XX shows a quadratic power dependence. This suggests the assignment of peaks X and XX to the excitonic ground state and the bi-exciton, respectively [87-88]. As shown in Fig. 5.13, the linewidth of a single InAs QD is around 1 meV and this value is very similar to another report [89]. The sample was measured at several points at a low excitation power, and about 20 spectra were observed. The narrowest observed spectral linewidth is about 60 μeV (FWHM). State filling effect easily occurs when the excitation power is increased, since only the small number of excitons can be accommodated in the small dot structure, resulting in broader PL spectra obtained at higher excitation powers [90]. Broadening caused by phonons is expected to be negligible in that case, since the population of phonons is very low at 3.8 K [91].

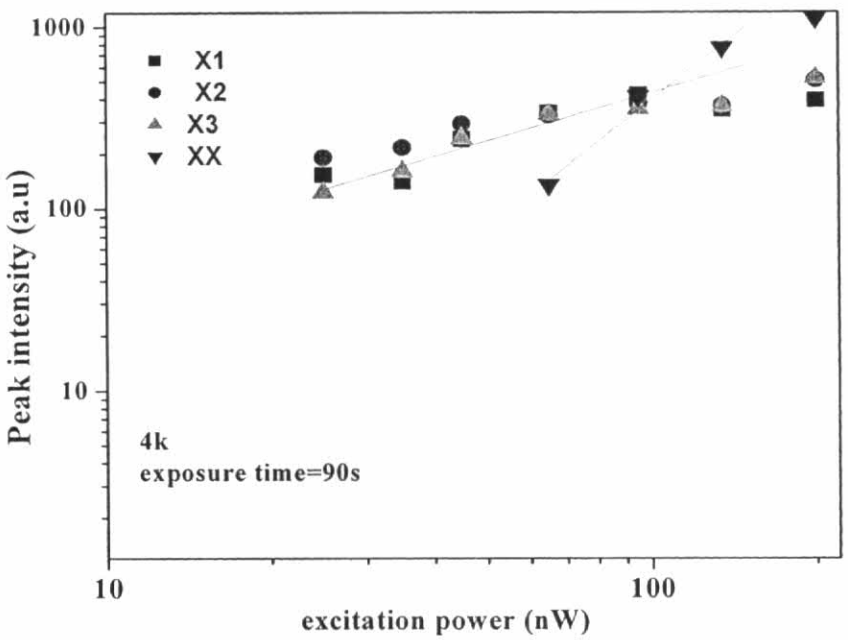

Figure 5.13 Excitation-power-dependent single-dot spectroscopy of exciton state and bi-exciton state from single-dot spectroscopy measured at 4 K. The exposure time to measure the optical signal the sample was 90 s.

The polarization-resolved PL measurements were made with a linear polarizer and a λ/2-waveplate inserted between the microscope and the spectrometer. The polarizer was rotated to maximize the grating efficiency of the spectrometer. The waveplate was then rotated in steps of 10° each. The two peaks are thus polarized in orthogonal directions. The energy split between 27 μeV and linear polarization is around 16%, as seen in Fig. 5.14. Theoretical results and some experimental results showed that the fine structure splitting and the linear polarization characteristic come from the elongation of the individual QDs(in the bi-QDMs) [92-94].

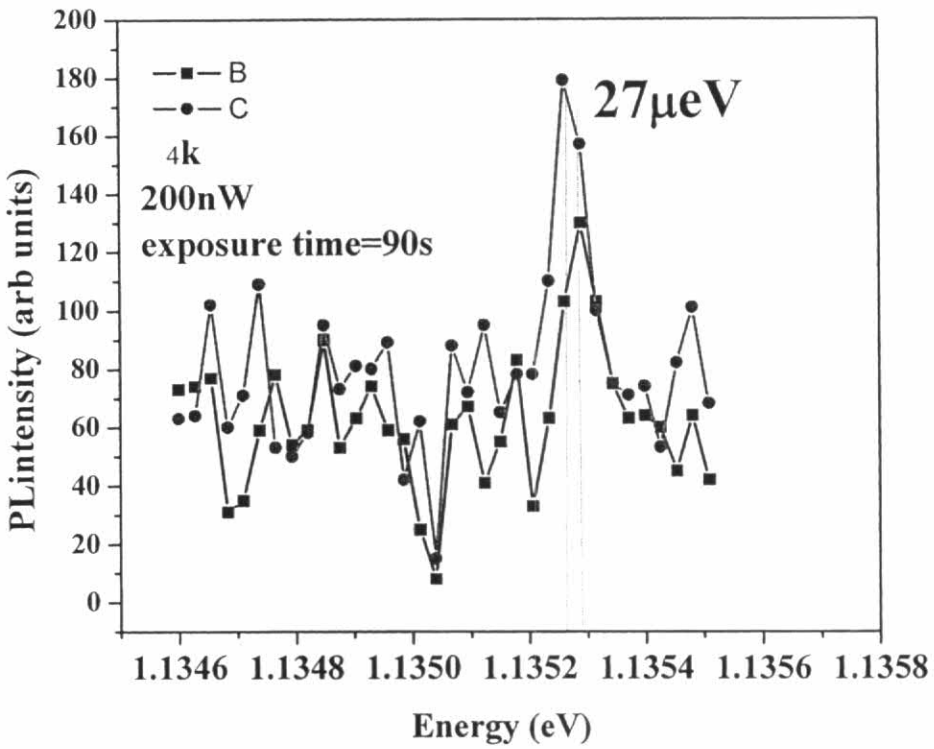

Figure 5.14 Polarization spectroscopy of single QDs in bi-QDMs. Fine structure splitting and the polarization characteristic were observed at 1.1352 eV.

5.2.3 Linearly Aligned Quantum Dots

5.2.3.1 Sample 0434 (Sample A)

This sample was used for our first optical characterization of linearly aligned quantum dots [95] . This sample has quantum dots aligned along the $[1\bar{1}0]$ direction (the alignment on average is about 500 nm long). The dots were grown by molecular-beam epitaxy on a [001] GaAs semi-insulating substrate using the thin-capping-and-regrowth process. After growing InAs QDs at 500°C, the substrate temperature was ramped down to 470°C and partially-capped with GaAs for 6 ML and then regrown with InAs QDs for 0.6 ML at the same temperature. After repeating the thin-capping-and-regrowth process for 3 cycles, 500 nm long aligned quantum dots were obtained on the nano-template as shown in Fig 5.15. For optical characterization, 100-nm capping was grown on the top of the sample.

In order to confirm the structure of the QDs, the surface morphology of the QD sample was observed under an atomic-force microscope (AFM). An AFM image of the nano-template is shown in Fig. 5.15, and that of linearly aligned quantum dots is shown in Fig. 5.16. The average size of the quantum dot is 60-80 nm and the height is about 3-4 nm.

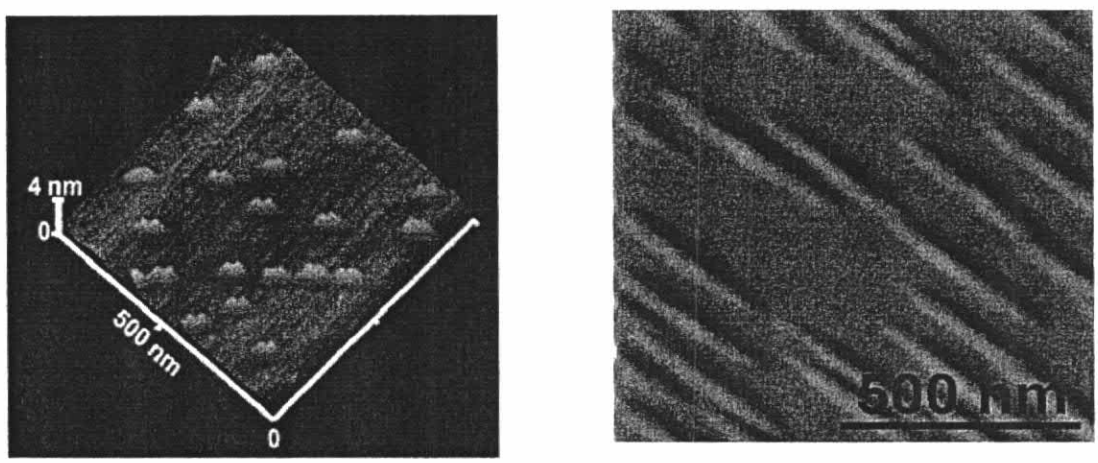

(a) (b)

Figure 5.15 AFM images of (a) a camel-like structure created as a result of thin-capping and regrowing over as-grown QDs, (b) nano-template for aligned quantum dots with an average length of 0.5 μm. (Suraprapapich *et al.*, 2005)

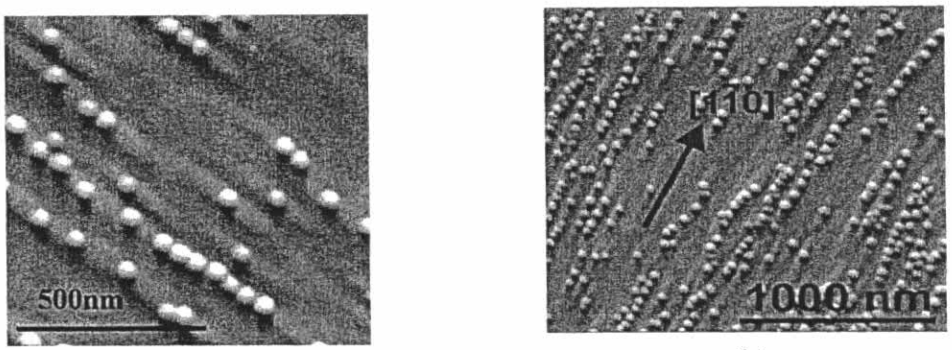

(a) (b)

Figure 5.16 AFM images of Sample A: (a) 500×500 nm^2, (b) 1×1 μm^2. (Suraprapapich et *al.*, 2005)

According to the AFM images, it was found that all QDs aligned along the [1$\bar{1}$0] crystallographic direction, but the alignment of the chained QDs was not perfect. Some parts of the chained QDs were closely packed together. The lateral spacing between one dot and another depends on the position of the sample.

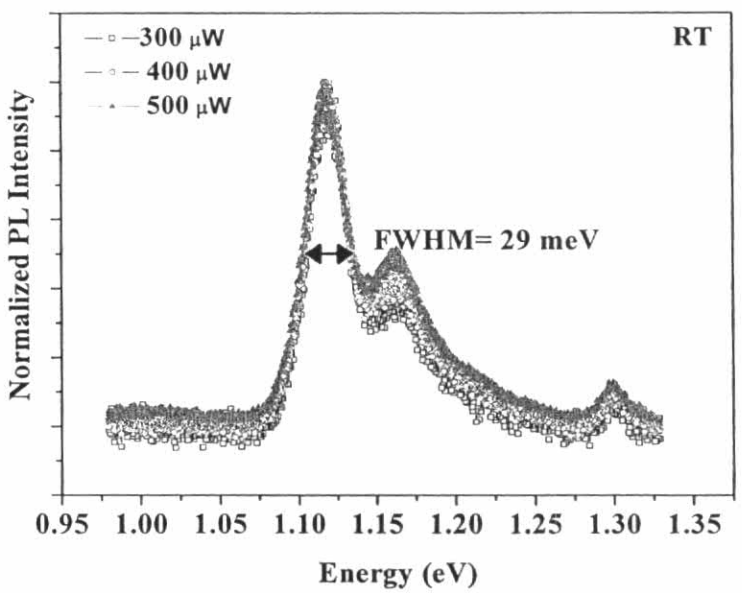

Figure 5.17 Room-temperature PL spectra of Sample A: Two peaks appeared and the third peak at 1.3 eV came from the wetting layer.

Figure 5.17 shows the room-temperature PL measurement. Two distinct emission features can be observed from the PL spectrum. The peak position difference between the main peak and shoulder peak in the figure is about 45 meV.

There are three possibilities to decide upon the origin of the lower peak at the higher energy side. It may come from the quantum dots with different sizes or the excited state of the quantum dots. Since the lower peak occurs in the higher energy level region, it may also come from the wetting layer. According to the AFM image, the size of the QD is almost uniform. To confirm the origin of the lower peak, the excitation-power-dependent photoluminescence was observed, as shown in Fig. 5.17. When the excitation power was increased, the peak height ratio between the lower peak and the main peak increased as well. If the lower peak came from the dots with different sizes, the peak intensity ratio would have been constant regardless of the excitation power [96]. Accordingly, the assumption that the lower peak corresponds to the transition between the second quantum levels can also account for the behavior of the excitation-power-dependent-PL intensity ratio change. From this result, it may be concluded that the lower peak comes from the first excited state of the quantum dots, and the smaller peak at 1.30 eV comes from the wetting layer of quantum dots.

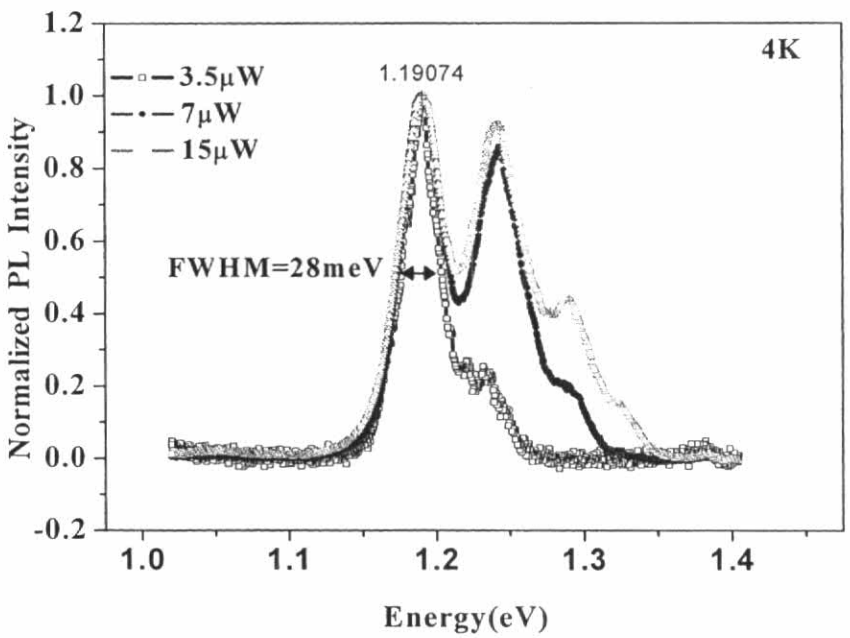

Figure 5.18 Low-temperature PL spectra of Sample A (4 K).

Figure 5.18 shows the low-temperature (4 K) PL measurement. The peak is shifted to the higher energy side with respect to the room-temperature PL spectra. The full width at half maximum at low-temperature measurement of 28 meV is not different from the room-temperature measurement. The quality of sample was good, and the linewidth broadening did not come from the defect or other effects, like the thermal effect, but comes from the intrinsic property of the dot-size inhomogeneity.

5.2.3.2 Sample 070081(Sample C)

On this sample, the length of alignment of quantum dots is about 1 μm. The dots were grown by molecular-beam epitaxy on a [001] GaAs substrate using the thin-capping-and-regrowth process, similar to Sample A, but the capping thickness was modified in the second cycle. After growing InAs QDs at 500 °C, the substrate temperature was ramped down to 470 °C and partially capped with GaAs for 6 ML and regrown with InAs QDs for 0.6 ML at the same temperature. After that 35 ML of GaAs capping was deposited on the QDs, and 0.6 ML of QDs was grown on it. Then, 6ML of GaAs was capped on top, and as a final step, 0.6 ML of QDs was finally grown on it.

In order to confirm the structure of the QDs, the surface morphology of the QD sample was observed under an AFM. From the AFM image of the Sample C, shown in Fig. 5.19(a), it was found that these QDs align in the [1$\bar{1}$0] crystallographic direction. The average size of the quantum dots is 60-80 nm and the height is about 3-4 nm.

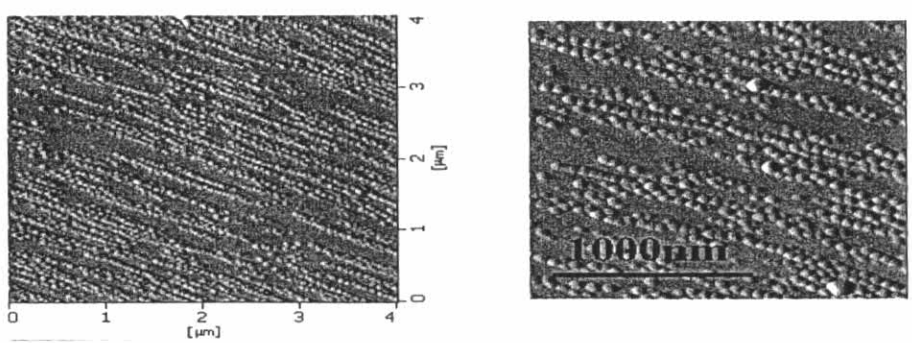

(a) (b)

Figure 5.19 AFM images of Sample C: (a) 4×4 μm^2, (b) 1×1 μm^2. The average alignment length is 1 μm. (Suraprapapich *et al.*, 2007)

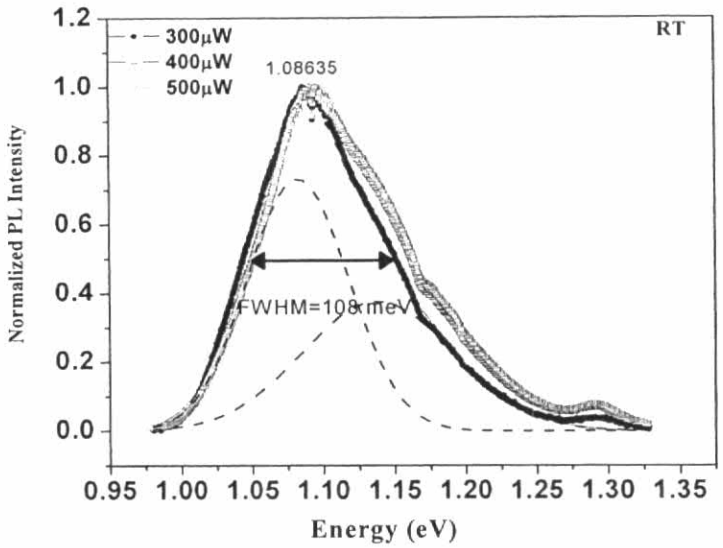

Figure 5.20 Room-temperature PL spectra of Sample C.

Figure 5.20 shows the room-temperature PL measurement. Broad PL emission features were observed with a peak at 1.08 eV in the PL spectrum. The full width at half maximum was about 108 meV.

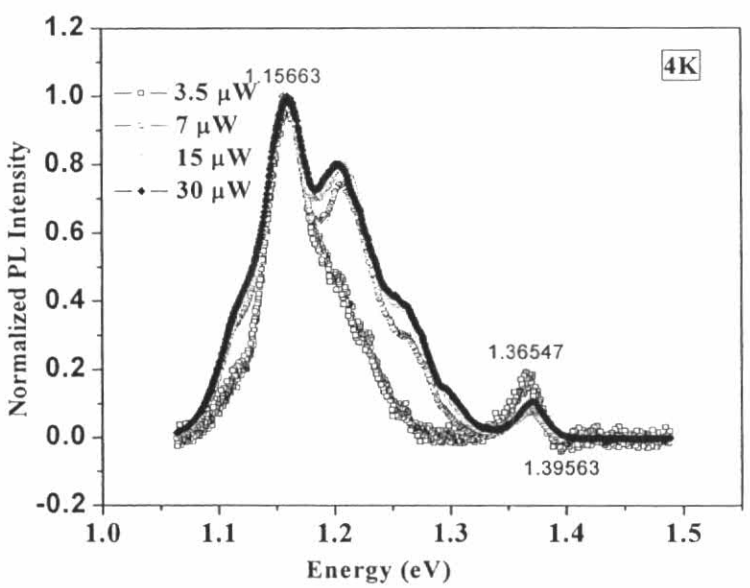

Figure 5.21 Low-temperature micro-PL spectra of Sample C.

For a low-temperature measurement, the shape of the spectrum is different from that obtained at the room-temperature. The full width half maximum was reduced to 58 meV, compared with 108 meV at room temperature. Larger linewidths at room-temperature may be attributed to some defects in the sample.

5.2.3.3 Sample 070080 (Sample B)

The length of alignment of quantum dots on this sample is around 1μm. The dots were grown by molecular-beam epitaxy on a [001] GaAs substrate using the thin-capping-and-regrowth process similar to the two previous samples. After growing InAs QDs at 500°C, the substrate temperature was ramped down to 470°C and partially-capped with GaAs for 6 ML and regrown with InAs QDs for 0.6 ML at the same temperature. After that 6 ML of GaAs capping was deposited on the QDs at 500°C and then 0.6 ML of QDs was grown on it at 470 °C. The thin-capping-and-regrowth process was repeated for only two cycles and the capping temperature modification was done in first cycle.

Like the previous samples, the alignments of the dots are directed along the $[1\bar{1}0]$ direction. The average size of the quantum dots is around 60-80 nm and the height is about 3-4 nm.

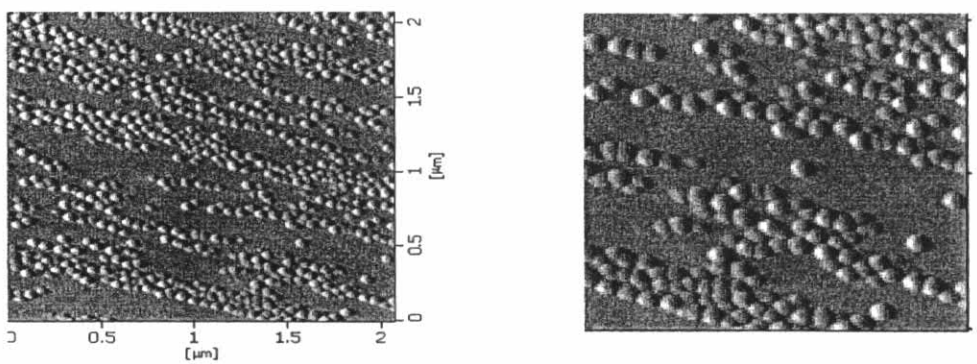

Figure 5.22 AFM images of Sample B: (a) 2 × 2 μm^2 (b) 1 × 1 μm^2 for aligned quantum dots. The average length is 1 μm. (Suraprapapich *et al.*, 2007)

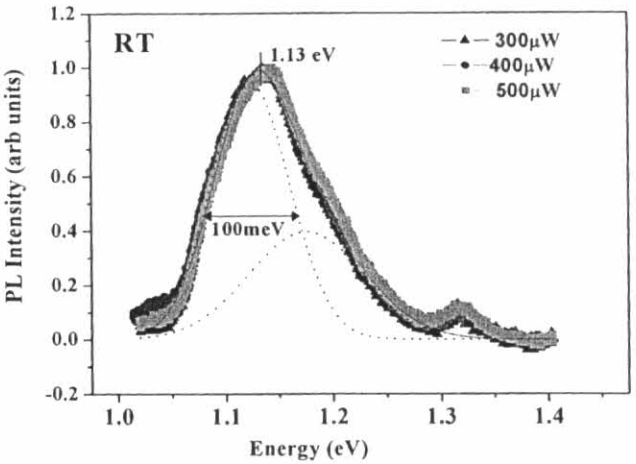

Figure 5.23 Room-temperature micro-PL spectra of Sample B.

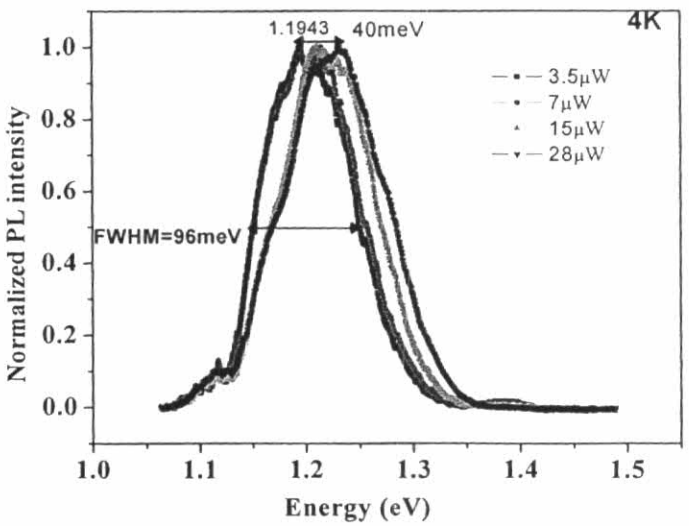

Figure 5.24 Low-temperature micro-PL spectra of Sample B (4K).

Figure 5.23 shows the room-temperature PL measurement. Broad PL emission features were observed with a peak at 1.13 eV in the PL spectrum. The full width at half maximum was about 100 meV. For a low-temperature measurement as shown in Fig. 5.24, the shapes of the spectra are not different from that obtained at the room-temperature. The full width half maximum was reduced to 96 meV compared with 100 meV at room temperature. Lager linewidths at room temperature may not be attributed to some defects in the sample but may come from the size inhomogeneity of QDs. Clear blue shifts were observed both for at room- and low-temperature measurements when the excitation power was increased.

5.2.3.4 Comparison of Three Laterally Aligned QD Structures and the Effects of Growth Parameters on Their Optical Properties

Table 5.2: Summary of growth parameters for three laterally aligned QD samples.

Structure	Sample A		Sample B		Sample C	
	Thick:	Temp:	Thick:	Temp:	Thick:	Temp:
GaAs (001) substrate	-	-	-	-	-	-
GaAs buffer layer	400 nm	580 °C	400 nm	580 °C	400 nm	580 °C
InAs as-grown QDs	1.8 ML	500 °C	1.8 ML	500 °C	1.8 ML	500 °C
First-cycle GaAs thin capping	6 ML	470 °C	6 ML	470 °C	6 ML	470 °C
Regrown InAs QDs	0.6 ML	500 °C	0.6 ML	470 °C	0.6 ML	500 °C
Second-cycle GaAs thin capping	6 ML	470 °C	6 ML	470 °C	35 ML	500 °C
Regrown InAs QDs	0.6 ML	500 °C	0.6 ML	500 °C	0.6 ML	500 °C
Third-cycle GaAs thin capping	6 ML	470 °C			6 ML	580 °C
Regrown InAs QDs	0.6 ML	500 °C			0.6 ML	500 °C

Table 5.3: Summary of PL of three laterally aligned QD Samples measured at room and low temperatures.

Parameters	Peak Energy (eV)		FWHM (meV)	
Temperatures	RT	4 K	RT	4 K
Sample A	1.12	1.19	29	28
Sample B	1.13	1.19	100	96
Sample C	1.08	1.16	90	58

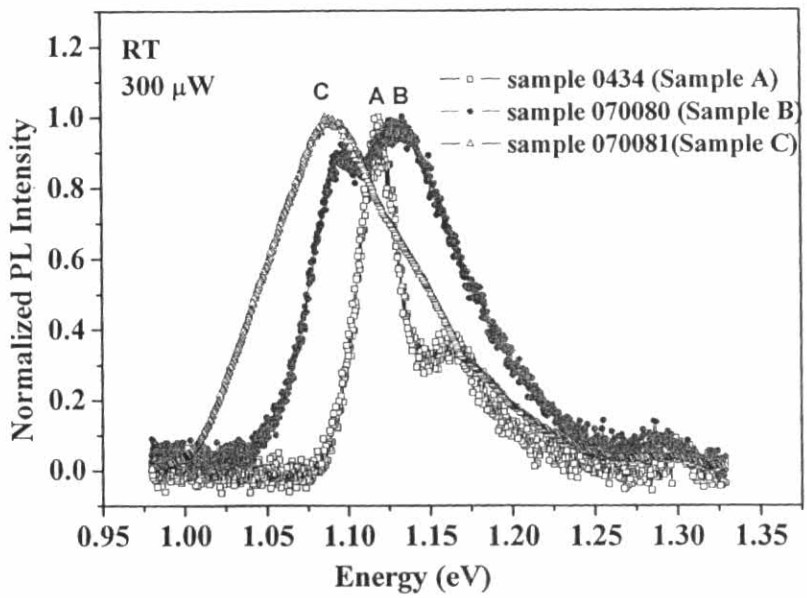

Figure 5.25 Comparison between room-temperature micro-PL spectra of Sample A, Sample B, and Sample C. The excitation power was held at 300 μW.

Room-temperature PL emissions from the three samples were observed around 1.1 eV and intense PL emissions imply improved confinement of InAs exciton and low defect density. These structures have good optical quality and can be utilized as a light emitting source at room temperature. PL emission from wetting layer was also observed around 1.3 eV in the three samples. All spectra are normalized to their maximum intensity value. Among these samples, the dot size homogeneity is the best in Sample A as seen from the narrowest linewidth out of the three samples of 29 meV (full width at half maximum). Also the emission intensity of Sample A was four times higher than that of the other two samples. Some modification of the growth process results in the dot size fluctuation for Samples B and C. Broader linewidth of 120 eV for Sample B and 110 meV for Sample C were observed. The PL spectra were broader in the higher energy side when the excitation power was increased. Each spectrum may be deconvoluted into two Gaussian peaks and the linewidth of the first peak is around 100 meV for Sample B and 90 meV for Sample C. The broader linewidth for higher excitation power indicates that state filling effect involves in this mechanism [96]. The distinct peak shift to the lower energy side occurs for the sample C; this is probably caused by the size of the QDs on this sample being larger than those on the other two samples due to some modification of the thin-capping-and-

regrowth process. Those changes may cause the chain of the QDs longer as well as more dot size inhomogeneity. Evidence for the dot size inhomogeneity and longer alignments were observed from the AFM images of Sample B and C.

For comparing the power-dependent PL of the three samples at low temperature (4 K), the samples were excited with the same source of laser excitation as the room temperature measurement. Concentrating initially on the shape of the three samples, different power dependence was observed. The PL peak was shifted into the higher energy level (shorter wavelength) compared with the room temperature measurements, as expected. But the linewidth and shape of the PL spectra for three samples were not strongly sensitive to the measurement temperature. In particular, they are almost the same as those obtained from the room temperature measurements. The broadening behavior of the PL spectra originally came from the size fluctuation of QDs on the samples. For sample A, the inter-dot coupling between the aligned QDs is not strong. There is no inter-dot carrier transport between one dot and another. Carriers are only captured and recombine in the QDs which give rise to the photoluminescence. Because of the random carrier capturing and recombination process, all the QDs contribute equally to the PL. When the ground states are fully occupied, the emission from the first excited state occurs [97]. This behavior was clearly observed in room and low-temperature measurements of the Sample A when the excitation power was increased.

As can be seen from Fig. 5.18 and 5.21, almost no change in the emission peak energy for Sample A and C occur. Distinct blue shift and broadening to the higher energy side for Sample B were observed when the laser excitation power was increased in room-temperature and low-temperature measurements as shown in Fig. 5.23 and Fig. 5.24. A possible reason is that optical transition with higher energy levels takes part in this peak shift. Dot size inhomogeneity means there are many sizes of QDs along the chain. At low excitation power, the photoexcited carriers are distributed in the barrier and try to find the lowest energy minimum (which is in larger QDs), recombine there, and emit photoluminescence. When the excitation power is increased, larger quantum dots are filled with carriers. This situation prevents the transferring of carriers from smaller to larger dots, and luminescence from the smaller QDs starts to appear. The whole emission came from all QDs and, as a result, PL

emission with shift to the higher energy (blue shift) and broadening in the higher energy side was observed [98].

The PL peak for Sample C which was observed at the lower energy side both at room temperature and at low temperature (4 K) reveals that not only the larger dot size but also the coupling effect involve in this peak shift compared with the other two samples. Due to interaction of closely packed QDs in the alignment, the ground state energy levels split into bonding and anti-bonding states. The PL emission may come from the ground bonding state [99]. This effect probably caused Sample C to radiate luminescence at a lower energy compared with Sample A and B. However, the population of the lower-energy dots and higher-energy dots are probably not much different, and so the blue shift could not be seen clearly at the low temperature. But for room-temperature measurement, a slight shift to the higher energy side and a broadening behavior could be seen. Therefore, coupling effect in Sample C was not obvious from the excitation-power-dependent PL measurement. The linewidth of 58 meV and the peak shift to the lower energy side for Sample C reveals that the average dot size is larger and more homogeneous compared with Sample B.

5.2.3.5 Polarization-Resolved PL Measurements of Linearly Aligned QDs

The polarization-resolved PL spectra at room temperature and low temperature were measured for the three samples. The results are shown in Fig. 5.26. At RT, the PD of the Sample A was 12%. The anisotropy was almost constant over the QD region (around 1.1 eV), indicating that the QDs in the Sample A have uniform shape, homogeneous size and constant strain distributions. At 4K, the PD was almost 14%. The results for the room temperature and 4 K measurement are not much different, which is within the error of the setup. Polarization property of Sample A does not depend on the measurement temperature, and thus PD for this sample may come from intrinsic (size and shape) properties of QDs.

For Sample B and C, the PD at room increased to about 15% which was probably caused by the longer alignment and the shape anisotropy of QDs. The PD was not constant throughout the whole energy spectrum, however. It decreased into the higher energy side because of the size fluctuation of the QDs on the sample. Larger quantum dots with lower energy levels exhibit higher polarization degrees.

When the temperature was decreased from room temperature to 4 K, the PD for both samples increased to approximately 30% (see Fig. 5.26).

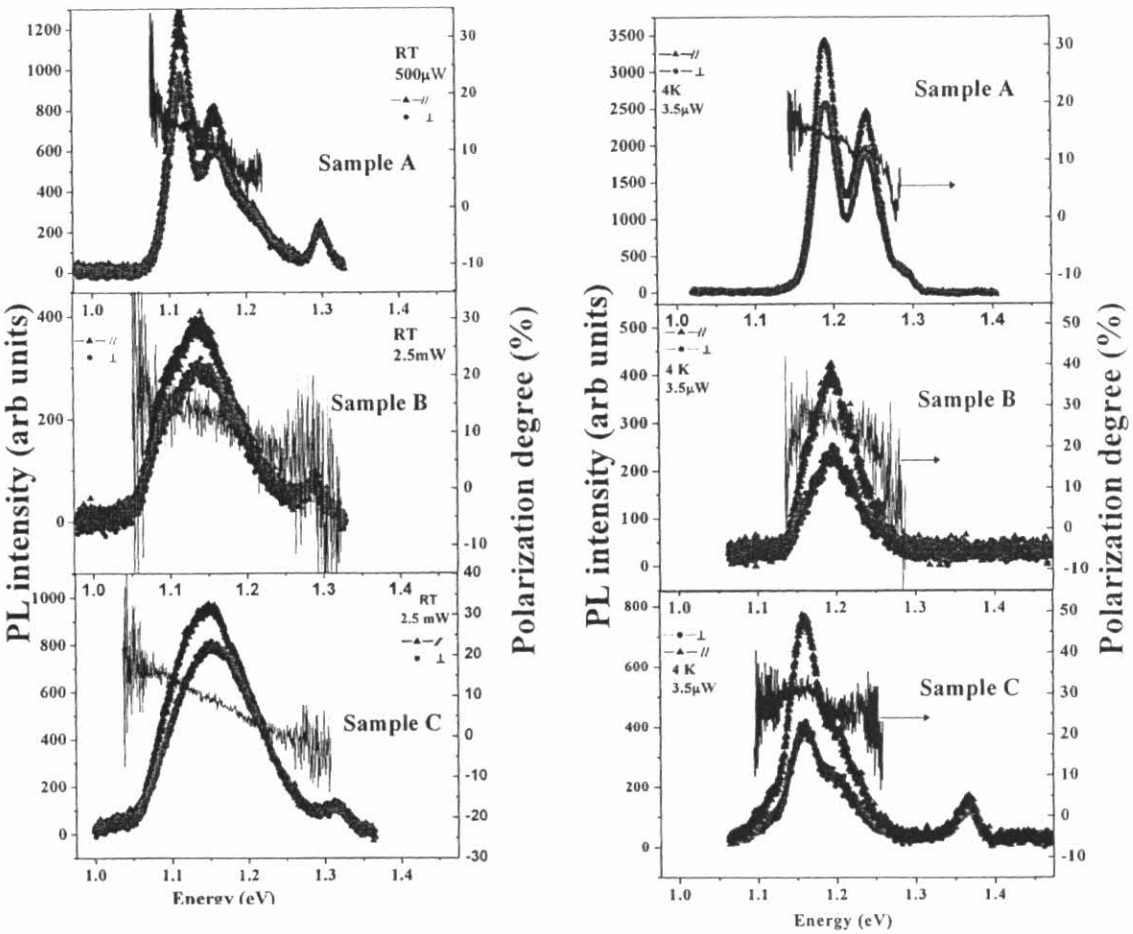

Figure 5.26 Comparison between room-temperature and low-temperature polarized micro-PL spectra for Sample A, Sample B, and Sample C.

The temperature-dependent PD was also measured for Samples B and C. The PD of these two samples strongly depends on the environmental effect. To investigate this behavior more carefully, a measurement was done at 70 K and the excitation power was held at 3.5 μW. The results are shown in Fig. 5.27. Carrier coupling effect and longer alignment of QDs in these two samples (Sample B and C) compare with the shorter alignment QDs in the Sample A. The overlapping of the wavefunctions caused by the QD coupling behavior gives rise to the stronger PD for these two samples. At very low temperatures, the localized and unoverlapped wavefunctions result in a small value of PD. When the temperature was increased to 70 K, the carrier coupling was stronger because of the thermalization effect. This 1D quantum-wire behavior at 70 K

thus gave rise to a stronger PD. The mechanism of decreasing of PD at room temperature is still not clear. One possible reason might be due to the thermal delocalization of carriers from the 1D quantum-wire state to the 2D quantum-well state with increasing temperature. When the temperature was high enough, the localized carriers would obtain enough energy to overcome the 1D like confinement of the lateral potential and move easily within the whole 2D quantum well, which causes a decrease in PD at high temperatures. But in this case, the energy difference between QD state and wetting layer (2D well) is high enough to jump the carrier from the QDs to wetting layer. This mechanism at reducing PD at higher temperature is still unclear. In summary the carrier diffusion to the neighborhood QDs in the sample A was not as strong as in the other two simples, and thus the polarization degrees at low and room temperatures are not much different.

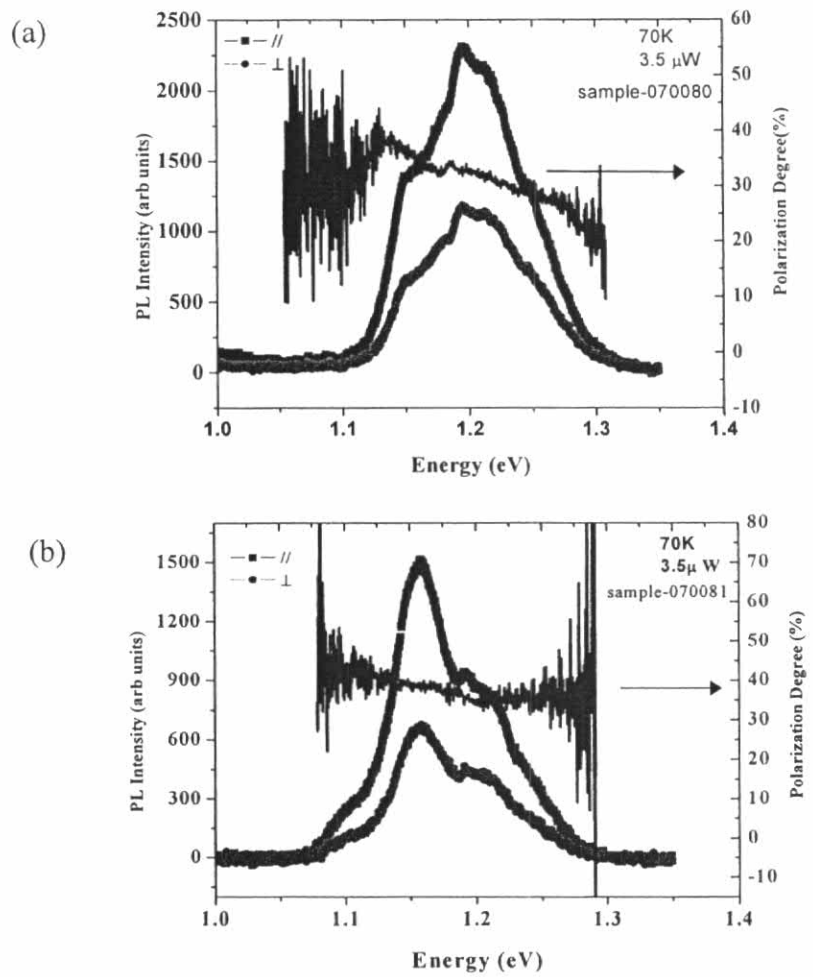

Figure 5.27 Comparison between polarized micro-PL spectra measured at 70 K of (a) Sample B, and (b) Sample C. The excitation power was held at 3.5μW.

Table 5.4: Summary of linear polarization degree versus temperature for Sample A, Sample B, and Sample C.

Temperature	4 K	70 K	RT
Sample A	13%	15%	11%
Sample B	28%	33%	14%
Sample C	30%	37%	14%

5.3 Optical Characterization of QDs on a Cross-Hatch Virtual Substrate

In this section, the optical characterization of aligned QDs on a cross-hatch pattern is discussed. In the growth of QDs on a cross-hatch, a virtual substrate of a partially-relaxed layer was used as a template, on which ordered QDs were then grown [100]. In an epitaxial growth of heterostructures, a strain is accompanied in the epitaxial layer due to the difference in the lattice parameters of the substrate and the epilayer. When the epilayer thickness is greater than a certain critical value, 3D islands are formed. But in small lattice-matched systems (<2%), the growth occurs layer-by-layer via a step flow mechanism, and 60° dislocations are nucleated and can thread to the epilayer surface, as a results in non-flat (undulating) surface morphology. This surface morphology caused by presence of a network of dislocations is known as a "cross hatch", of which as-grown QDs are grown on top.

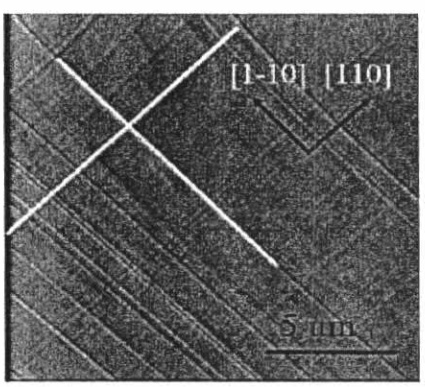

Figure 5.28 AFM image of a cross-hatch virtual substrate before QDs were grown on it. (C. C. Thet *et al.*, 2007)

5.3.1 Sample 0607 (Sample X1)

The first sample containing QDs on cross hatches studied here was grown on a [001] GaAs substrate by MBE. A 300 nm GaAs buffer layer was deposited first at 580°C, followed by the 50 nm of $In_{0.15}Ga_{0.85}As$ after reducing the substrate temperature to 500°C. Then the substrate temperature was reduced to 470°C and 0.8 ML of QDs was grown on the InGaAs layer. Finally QDs on the virtual substrate were covered with the 0.1-μm un-doped GaAs capping layer for PL measurements.

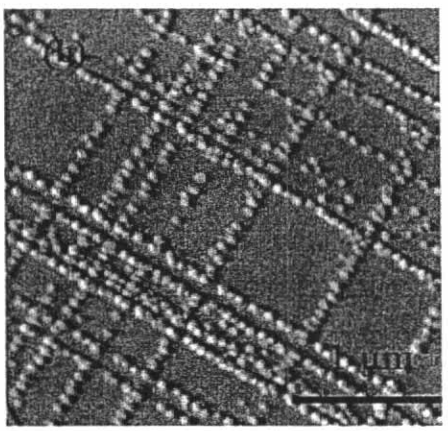

Figure 5.29 AFM image of QDs on a cross-hatch pattern. 50nm of $In_{0.15}Ga_{0.85}As$ layer was used for the cross-hatch pattern. Because of the well-patterned substrate, QDs were well aligned. (C. C. Thet *et al.*, 2007)

Table 5.5: Dimensions of five representative QDs on a cross-hatch pattern (Sample X) from SEM measurement.

Direction	QD1	QD2	QD3	QD4	QD5
[1$\bar{1}$0] Length (nm)	35	37	31	27	28
[110] Width (nm)	28	31	23	18	20

Table 5.6: Distance between one QD and its neighbor on the cross-hatch pattern (Sample X) from SEM measurements at five locations on the sample.

Direction	point1	point2	point3	point4	point5
[1$\bar{1}$0] Length (nm)	12.09	11.72	8.593	9.21	6.5
[110] Length (nm)	59	42	59.3	53	53

Figure 5.29 (a) shows the surface morphology of the QDs under an AFM image. According to the AFM image, the QDs aligned in the [110] and the $[1\bar{1}0]$ directions. Analysis of SEM images obtained at various sample orientations shows that the QDs have an average diameter of 31 nm in the $[1\bar{1}0]$ direction and 24 nm in the [110] direction. The average height of the QDs was 3 nm. The average shape anisotropy due to elongation of the InAs islands was thus $L[1\bar{1}0]/L[110] = 1.3$, where L is the maximum length of the island along the corresponding [110] and $[1\bar{1}0]$ directions. The shape of QDs studied in this work was slightly ellipsoidal, and the axis of elongation of all QDs tends to the $[1\bar{1}0]$ direction.

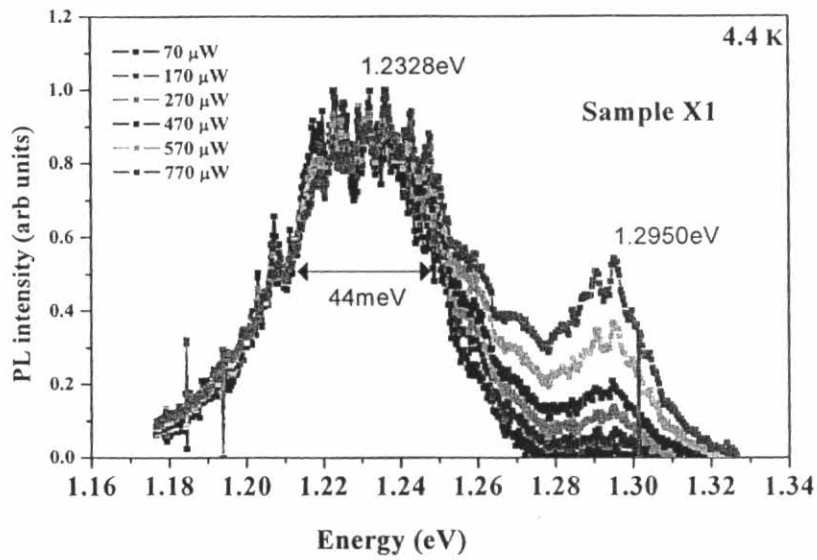

Figure 5.30 Excitation-power-dependent PL spectra of QDs on the cross-hatch (Sample X1) measured at 4.4 K.

Figure 5.30 shows PL spectra of QDs on the cross hatch under the various excitation powers measured at 4.4 K. At a low excitation power, only one emission peak was observed at around 1.23 eV. When the excitation power was increased, the second peak which was luminescence from the excited state could be observed. According to the state filling effect, lower energy states will become saturated and a higher energy state will then begin to be populated if the excitation density is high enough. By deconvoluting these PL spectra with Gaussian fit, it was found that the separation between the ground-state and the excited-state peak was about 62 meV, and their full-width-at-half maximum ranges from 44 to 55 meV, arising from the QD size fluctuations.

5.3.2 Sample 0620 (Sample X2)

The second sample containing QDs on cross hatches was grown by using the same recipe as that of the previous sample (Sample X1), except that the thickness of $In_{0.15}Ga_{0.85}As$ cross-hatch layer was increased to 100 nm compared with 50 nm in Sample X1.

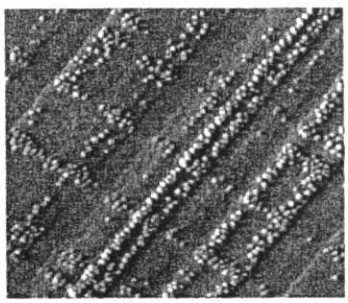

Figure 5.31 AFM image of QDs on a cross-hatch pattern. 100 nm of $In_{0.15}Ga_{0.85}As$ layer was used the for the cross-hatch pattern. Because of ill-patterned layer, the QDs were not well aligned. (C. C. Thet *et al.*, 2007)

The surface morphology of this sample was analyzed by using the AFM and the SEM images. According to AFM images, the QDs are aligned in the [110] and the $[1\bar{1}0]$ directions. Analysis of the SEM images obtained at various sample orientations revealed that QDs of the average diameter was about 31nm in the $[1\bar{1}0]$ direction and about 24 nm in the [110] direction (similar with the Sample X1). The average height of the QD was about 3 nm. Because of the thicker InGaAs (100 nm), the QDs on this sample were not aligned in the misfit dislocation lines and in some parts of the alignment, the QDs were located close to one another and appeared as groups, and the shape of all individual QDs appeared as almost ellipsoidal and all elongations tend to the $[1\bar{1}0]$ direction. Fig. 5.32 shows the PL spectra for various excitation powers obtained at 4.4 K. There were two peaks found for this sample (see Fig. 5.32 and 5.33). All peaks are normalized into first lower energy peak value. The peak at 1.18 eV came from the emission of QDs and the FWHM of this spectrum is 50 meV but the spectrum of higher energy peak at 1.32, with a narrower FWHM of 17

meV, intense emission peak than QDs peak, came from the InGaAs-cross-hatch layer which was resulted from the thicker layer of InGaAs.

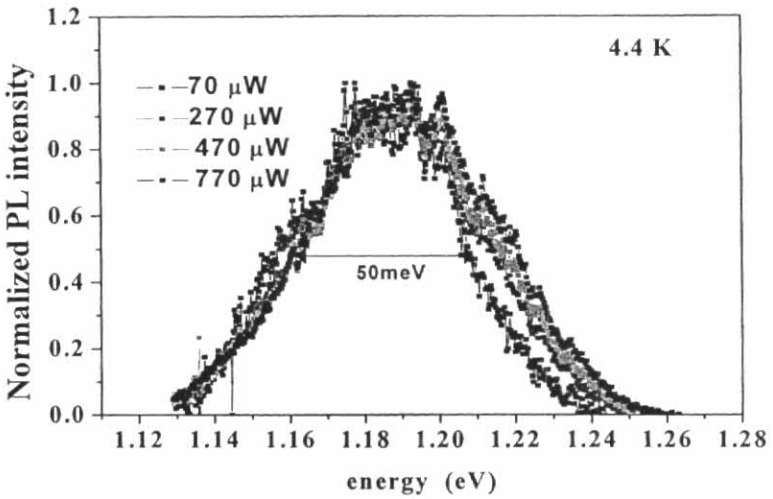

Figure 5.32 Excitation-power-dependent PL spectra of QDs on a cross hatch measured at 4.4 K (Sample X2).

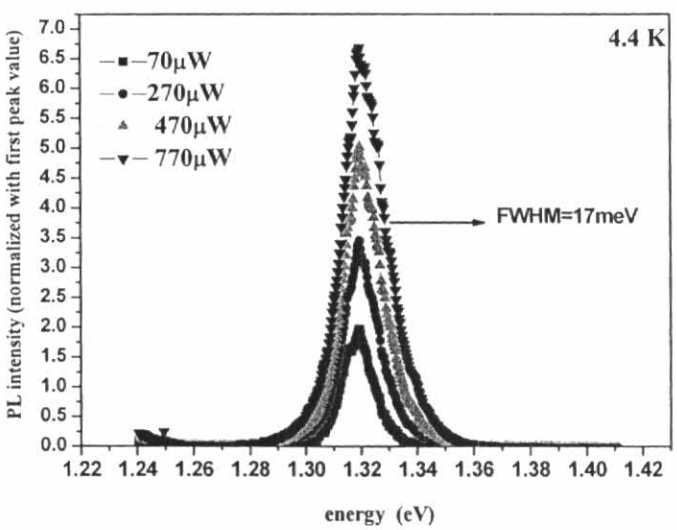

Figure 5.33 Power-dependent micro-PL spectra of Sample X2. The peaks were at 1.32 eV and the emission intensity was stronger than that emitted from the QDs and the linewidths of the spectra were small.

5.3.3 Polarization-Resolved PL Measurements

The polarization degree for both Samples X1 and X2 were measured by rotating a half-waveplate and fixing the polarizer in the optical setup.

5.3.3.1 Sample X1

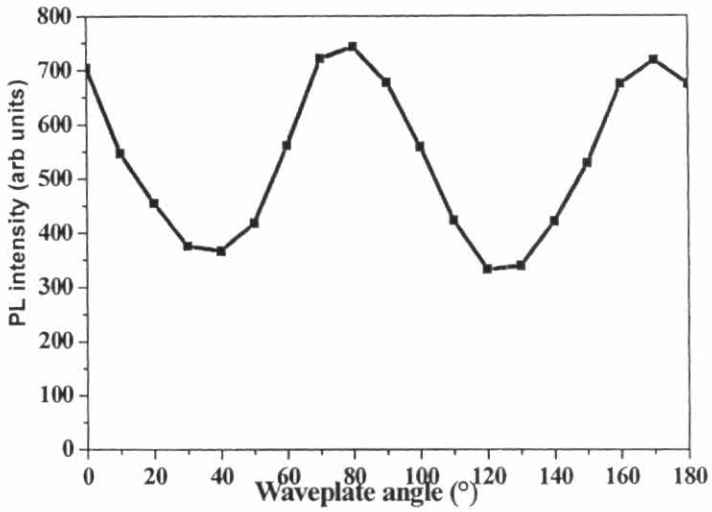

(a)

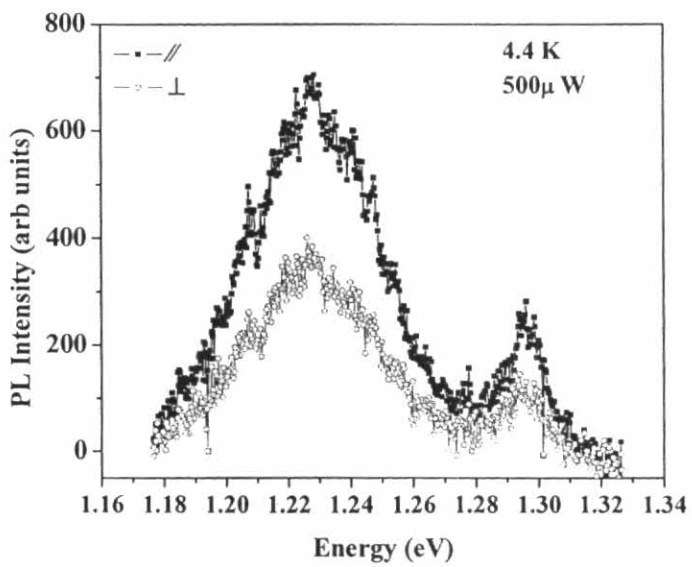

(b)

Figure 5.34 (a) Polarized-PL measurement result, which follows the Malus's law, and (b) polarized-PL spectra of Sample X1 measured at low temperature (4.4K).

Table 5.7: Polarization degree of Sample X1 measured at five different locations on the sample.

	Point 1	Point 2	Point 3	Point 4	Point 5
Polarization degree (%)	22%	20%	33%	14%	17%

5.3.3.2 Sample X2

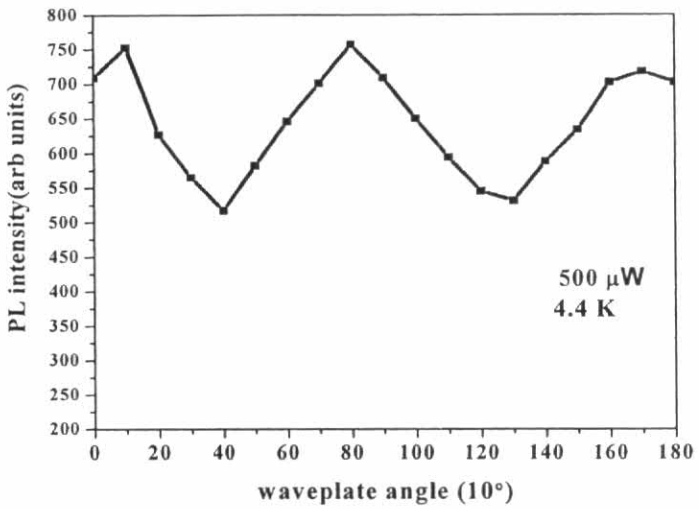

(a)

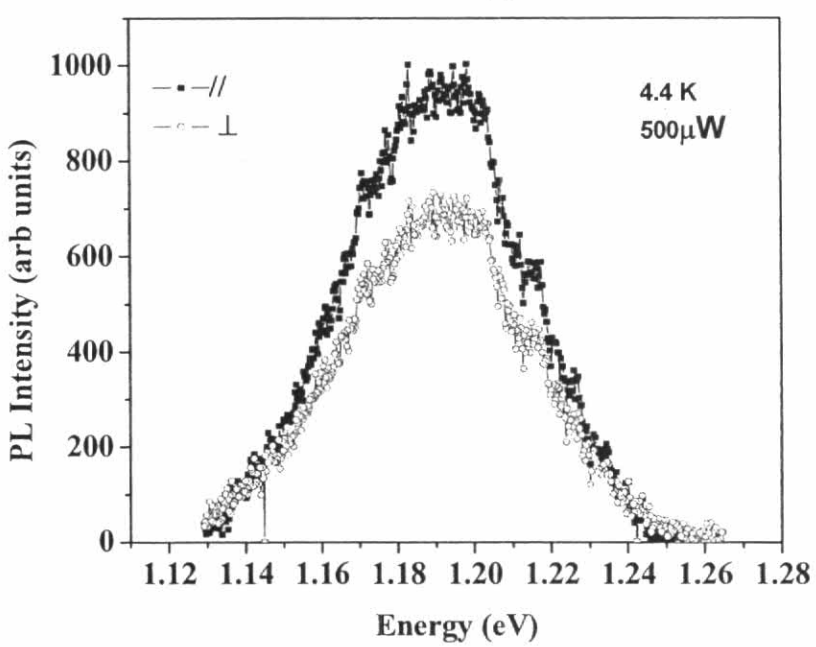

Figure 5.35 (a) Polarized-PL measurement result, which follows the Malus's law, and (b) Polarized-PL spectra of Sample X2 measured at low temperature (4.4 K)

The polarization property (PD) was observed from the PL of both samples. But the value of PD depends on the position on the sample. To find out the origin of the polarization behavior of the sample, the temperature-dependent PL was measured. Since the main interest was in the polarization property of aligned QDs, Sample X1 was chosen to be measured because its all QDs were located on the cross-hatch pattern and their alignment was good compare with Sample X2.

5.3.4 Temperature-Dependent PL Measurement of Sample X1

Temperature-dependent PL data from 10 to 130 K (Fig. 5.36 and Fig. 5.37) were also obtained while the incident excitation intensity was held constant at 100 μW. These emission energy peaks, which can be fitted by using the Varshni model $E(T) = E_0 - \frac{\alpha T^2}{T + \beta}$ where $E(T)$ and E_0 are the peak energies at T and 0 K, respectively, and α and β are constants [101]. Normally, the variation of the peak emission energy with temperature can be attributed to the effect of dilation of the lattice and of the electron-lattice interaction. The theoretical analysis shows that the results obtained follows the Varshni equation. The lower solid line in Fig. 5.37 is a curve fitted to the Varshni equation with E_0= 1.215 eV, and α = 3.37×10^{-4} eV/K and β = 93 K are the Varshni coefficients for the cross-hatch QDs. For the cross-hatch QD samples, the maximum red shift of 25 meV deviating from the Varshni equation might not be due to the carrier transferring from smaller quantum dots to the larger quantum dots as in the bi-QD samples because the interdot spacing between adjacent QDs on the cross-hatch sample was not close enough for the carrier transfer to occur, but might be due to the carrier scattering by phonons at high temperatures.

Temperature-dependence of the wavelength-wise integrated PL intensity of the cross-hatch QD luminescence is also shown in Fig. 5.37. The integrated PL intensity increases with temperature in the low temperature range and then monotonically decreases at higher temperatures. Above 130 K, the PL signal could not be detected even raising the higher excitation power. This is attributed to the defects such as cross-hatches themselves which could affect the optical efficiency due to non-radiative recombination near the quantum dots and cross-hatch pattern template [102-104]. In the lower temperature range, the integrated PL intensity increasing with temperature indicates that the process of carrier capture from the wetting layer or the barrier is

stronger than the process of carrier activation inside the QDs. At higher temperatures, the carrier activation is stronger than the carrier capture. In other words, when the temperature is increased, the carriers in the dots are thermalized and become activated into the dislocation line near the QDs. This layer capture the carriers diffused by the QDs and acted as the non-radiative recombination center. This non-radiative recombination process occurred in the dislocation near the QDs, which affects the optical properties of the QDs when the QDs are site-controlled by the misfit dislocations even if there is strong carrier confinement in QDs. Any defects and dislocations in the material will provide the non-radiative channel to quench the luminescence. Therefore, the intensity of the luminescence will be lessened, and after 130 K the luminescence is not detected.

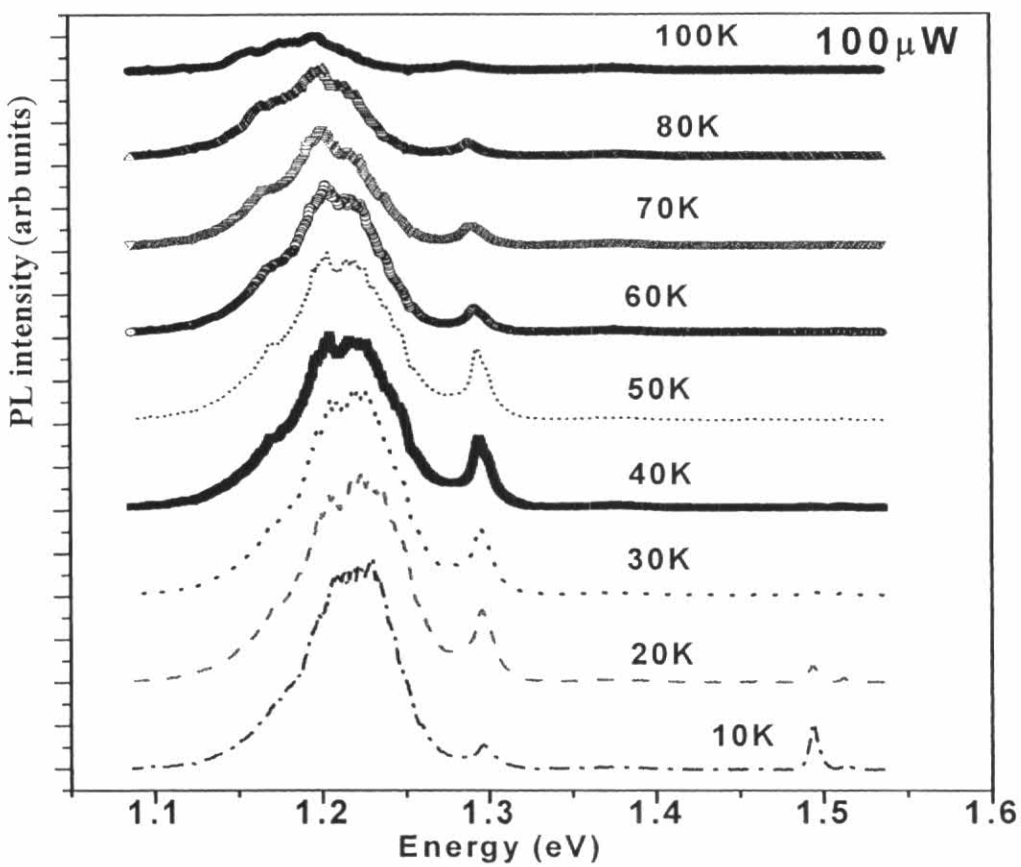

(a)

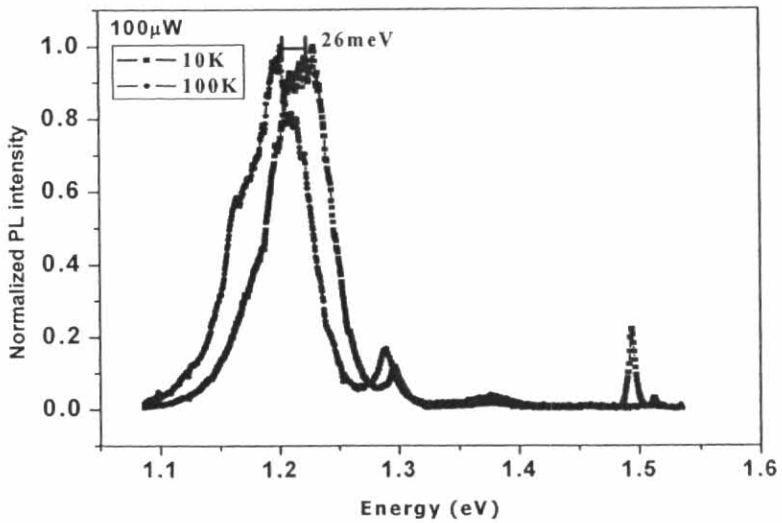

(b)

Figure 5.36 (a) Temperature-dependent PL spectra of Sample X1, and (b) peak shift caused by the effect of temperature is clearly be seen in the figure.

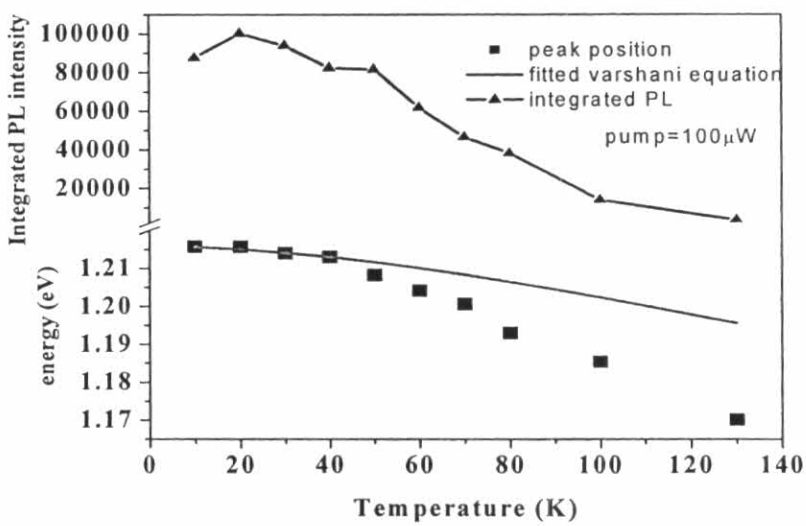

Figure 5.37 Temperature-dependent PL measurement result showing the integrated PL intensity and peak shift for Sample X1.

Finally, the polarized PL from QDs on the cross-hatch template was observed. Figure 5.38 (a) and (b) show the polarization-resolved PL spectra of QDs on the cross-hatch sample. At 6 K, the linear polarization $PD = (I_{max}-I_{min})/(I_{max}+I_{min})$ was 19%. The anisotropy dramatically decreased to the higher energy level, indicating that PD is larger in larger QDs (lower energy minimum) than smaller QDs (higher energy

minimum). This polarization anisotropy was attributed to elongation of individual quantum dots along the $[1\bar{1}0]$ direction as evident from the AFM and SEM results. The PD was investigated at various locations across the sample. The PD changed randomly when moving the excitation spot over the QD arrays. The polarization degree depends on the position of the sample. Five different locations on the sample were measured by micro-photoluminescence measurement. The value of PD ranges from 13 % to 20%.

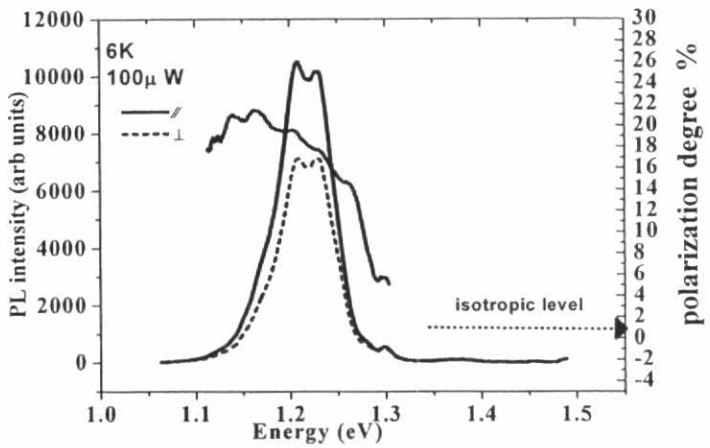

(a)

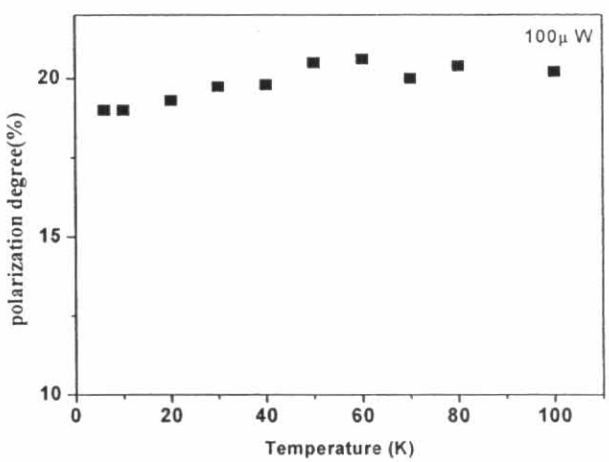

(b)

Figure 5.38 (a) Polarized PL spectra of QDs on the cross-hatch sample measured at 6 K, and (b) temperature-dependent polarization degree for Sample X1 (4 K to 130 K).

The PD ranging from 13% to 20% suggests that the distribution of the QDs on the array was inhomogeneous. Different values of PD at different locations could be explained by the fact that some parts of the alignment had the QDs located close together and the carriers that were photogenerated in the individual QDs were not isolated but correlated with those in the neighboring QDs along the $[1\bar{1}0]$ direction. To test this assumption, the temperature-and excitation-power-dependent polarization anisotropy was measured. A strong dependence of the polarization anisotropy on the excitation power and temperature would be expected if the polarization was caused by the carrier diffusion process. An excitation power dependence of the polarization anisotropy was indeed observed; at the excitation power of 16 μW, the polarization degree was 19.15% and the excitation power was increased to 100 μW, the PD decreased slightly to 19.13% on the same excitation spot on the sample, all performed at 10K .

In fact, temperature-dependent PD measurements showed that PD increased slightly with temperature (Fig. 5.38 (b)). Around 40 K and 50 K, the PD increased slightly and reaches a value of 21% and after that decreases to 19%, indicating that the PD manifested a saturation for temperature ranges between 40 and 130 K. This experimental finding demonstrates that the polarization anisotropy of the QD signal in PL spectroscopy is not only due to an oscillator strength asymmetry [105] but also small amount of effect from the carrier dynamics. To confirm this result, the SEM images of the QDs were carefully investigated. The average distance to the nearest neighbors QDs was 9.6 nm in the $[1\bar{1}0]$ direction and 55 nm in the [110] direction. The average distance between QDs in the $[1\bar{1}0]$ direction was closer than that in the [110] direction. In the latter there were no interacting electrons between the neighboring QDs. But in the former the QDs each had close neighbors, but the carrier diffusion between neighboring QDs was not strong. The polarization anisotropy for this sample was thus caused only by the shape and size effect of the QDs.

5.5 Overall Discussion

The following are the main results presented in this chapter:

1. First, randomly distributed InAs quantum dots and high-density QDs were measured as the reference samples for all measurements.

2. It was shown that randomly distributed InAs QDs and high-density QDs did not show any polarization degree, as expected, and some polarization of <4% might come from some error of the optics from the setup. These two samples did not follow the squared cosine rule (the Malus's law).

3. Interesting results could be seen from the binary-QD sample. The single-dot spectroscopy from this sample showed the fine structure splitting, so that the overall polarization characteristic from this sample came from the size anisotropy of individual QDs. But almost no polarization degree at room-temperature reveals that the polarization anisotropy of the individual QDs on the bi-QD sample was not strong. Temperature-dependent PD could be clearly observed for this sample. The PD strongly depended on the temperature. The carriers were localized in the QDs at low temperatures and the small amount of PD came from the shape anisotropy of QDs. At higher temperatures, the carriers became activated and tried to communicate with one another in the adjacent dots. Two QDs acted like a quantum wire which gives rise to a larger amount of PD. In the vicinity of room temperature, activated carriers might spill over the surrounding wetting layer and the quantum-wire-like behavior reduced, and thus the PD was reduced. The real mechanism of this is still unclear, however. Very close distance between the two QDs addresses an important quantum mechanical effect, and the strong emission intensity at room temperature from this structure make it having potential to be utilized in quantum cellular automata (QCA) and infrared photodetectors. However, the emission intensity was not as high as-grown QDs and linearly aligned QDs, and the relatively large FWHM value reveals that the dot size homogeneity was not good. For utilizing this structure in light emission device, some modifications to reduce defects and improved dot size homogeneity are needed.

4. Three samples of linearly aligned QDs were investigated. Measurement results show that optical properties of these samples depend on the growth parameters. Strong emission intensity at room temperature, temperature-insensitive FWHM, and

high polarization degree of these structures can be prosperous for future optoelectronic devices like QD laser with polarization characteristic incorporated. And quantum mechanical coupling between the QDs of these structures may be interesting result for QD infrared photodetectors.

5. QDs on the cross-hatches were observed and it was found that optical properties of these samples depend on the pattern of the QDs. The dislocation line may act as the non-radiative recombination center and affects the QD emission intensity. The emission intensity at room temperature was not observed and the emission intensity strongly depends on temperature. Degree of shape anisotropy of QDs was high and all individual QDs in the whole sample showed stronger degree of shape anisotropy. The shape of the QDs was large and the average distance between nearest QDs was 10 nm. Because of larger size and larger separation between the QDs, the quantum mechanical coupling between the QDs was not pronounced for this sample. The polarization degree of these structures may come from the shape anisotropy of the QDs. In addition, almost constant temperature-dependent PD confirms the results of the polarization measurements. Because of temperature-sensitive emission intensity, it is difficult to be utilized as light emission device. But long-range QDs are expected to be used in some electronic devices and the ordering nature of QDs is good to be used in photonic crystals. Also, large and high polarization degree of QDs can be used for polarization-sensitive switches. But some growth modification is needed for better device application if this kind of structure is used.